Progress In Electromagnetics Research C, Vol. 91, 197–211, 2019

MERR Inspired CPW Fed SSGF Antenna for Multiband Operations

Nirmala Jayarenjini[1, 2, *] and Cheruvathoor Unni[2]

Abstract—An Electric Ring Resonator (ERR) loaded Sierpinski Square Gasket Fractal (SSGF) antenna for multiple frequency band application is proposed, fabricated, and measured. The CPW-fed antenna consists of a Multi-mode Electric Ring Resonator (MERR) which is fixed on reverse side of the substrate and iterated Sierpinski gasket fractal derived from a square patch which is stamped on top of an FR4. Multi-bands can be obtained by placing a single multi-mode ERR beneath the CPW structure of the antenna. Each resonating frequency band can be easily tuned by properly changing the dimensions of the ERR structure. Instead of ERR's quasi-lumped capacitance, reconfigurability of the low, middle, and high frequency bands can be achieved by using a pair of Digital Variable Capacitors (DVCs) inserted into the middle of the ERR's rings corresponding to the chosen mode. The bandwidth is enhanced using four iterations of square radiating patch, modified feed line, and multi-mode electric ring resonator-loaded ground plane. More specifically, the impedance matching of the CPW fed antenna is improved by introducing transitions between the microstrip feed line and the Sierpinski square gasket. The numerical results show that the proposed antenna has good impedance bandwidth and radiation characteristics in the operating bands at 3.08/5.81/8.02/12.13/15.56 GHz which cover the frequency spectrum of WiMAX, WiFi/WLAN(IEEE 802.11a), IEEE 802.16e, X-band uplink, S/C/X/Ku and K band with return loss of better than 10 dB.

1. INTRODUCTION

Wireless communication industry poses systems capable of operating in multiple bands and requires antennas with small size, light weight, low profile, and can be easily integrated with other microwave components. Various applications use the lower end of UHF band while WLAN and UWB operate in the upper UHF band. Multiband antennas with frequency notched function are useful for wireless communications because a single antenna can cover several different frequency bands while decreasing noise interference at frequencies outside the selected band. Due to the wideband characteristics and ease of integration with MMICs, planar antennas with CPW (coplanar waveguide) feed have received much attention [5–9].

Due to inherent properties like small size, self-similarity, and multiband capability, fractal antennas are commonly employed to develop multiband antennas [11, 15]. A Sierpinski gasket monopole antenna was introduced by Puente et al. [14]. To translate into its electromagnetic behavior this popular antenna used the self-similarity properties of fractal shape. The classic Sierpinski gasket generated by Pascal triangle is a popular antenna using the self-similarity property of fractals [1–4]. By altering the radiating strip or ground flat and by utilizing dissimilar shapes, multiple band resonating modes can be achieved [18].

The combination of fractal concept and meta-materials confines the applications of the antenna to decrease the complexity and miniaturize antenna dimension. Metamaterial is an artificial homogeneous structure synthesized to display negative permeability and negative permittivity simultaneously [29].

Received 2 February 2019, Accepted 19 March 2019, Scheduled 1 April 2019
* Corresponding author: Nirmala Jayarenjini (jayarenj@gmail.com).
[1] Department of ECE, ACE College of Engineering, Thiruvananthapuram, Kerala 695027, India. [2] LBS Centre for Science and Technology, Thiruvananthapuram, Kerala 695033, India.

Split ring resonator (SRR) is one of the main elements of metamaterial [17, 27]. Negative permeability characteristics and bandwidth improvement can be achieved by the use of SRR [26]. Different SRR structures are reported in the literature such as Multiple Split Ring Resonator (MSRR), Labyrinth Resonator (LR), Spiral Resonator (SR), Broad Side Coupled Split Ring Resonator (BCSRR), and Non-Bianisotropic Split Ring Resonator (NBSRR) [10, 16]. Because of the resonant nature, the design of a compact radiating element for CPW-fed antennas and microstrip planar antennas can be employed by SRR.

In this article, a Sierpinski square gasket fractal patch (Top Side) and Multi-mode Electric Ring Resonator (MERR) (Flipside) antenna are projected for S-band/Non-coherent UWB — 2 to 4 GHz, WiFi/WLAN (IEEE 802.11a) — 5.18 to 5.87 GHz, X-band uplink — 8.02 to 8.5 GHz/10.28 GHz, Ku band downlink — 10.7–12.75 GHz, Ku band — 15.56 GHz. Sierpinski gasket fractal derived from a square patch is used. CPW feed is used with source and symmetry ground. The ERR resonance frequency with permittivity characteristics is also studied. The radiation characteristics of the antenna such as S_{11}, gain, VSWR, and impedance bandwidth are mandatory, and the characteristics depend on the entire operating frequency. The proposed antenna is designed, simulated, and optimized by using electromagnetic simulator software CST microwave studio.

2. ANTENNA DESIGN AND SIMULATED RESULTS

2.1. Antenna Geometry

A CPW-fed Sierpinski square gasket fractal patch configuration (top view) and Multi-mode Electric Ring Resonator (MERR) (Reverse view) are shown in Figures 1(a) and (b). The antenna is etched on

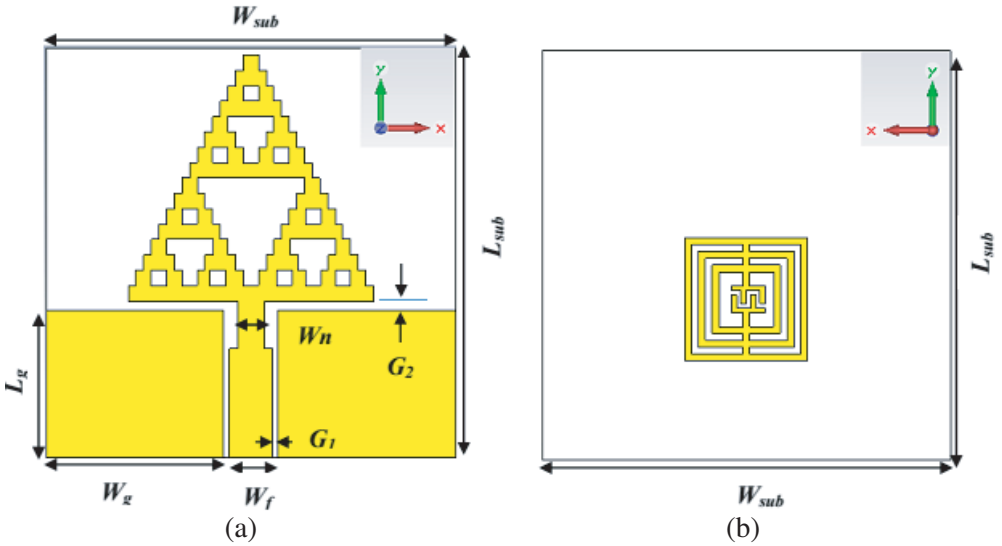

Figure 1. Geometry of CPW Fed Sierpinski square gasket fractal patch antenna [Top] and Multi-mode ERR [Bottom].

Table 1. Optimized dimensions of the designed antenna.

Parameters	Dimensions (mm)	Parameters	Dimensions (mm)
W_{sub}	30	W_f	3.2
L_{sub}	30	W_n	2
W_g	13	G_1	0.4
L_g	10.8	G_2	0.7

an FR-4 substrate having relative permittivity (ε_r) of 4.4, loss tangent ($\tan\delta$) of 0.02, and thickness of 1.6 mm. The overall dimension of substrate is 30 mm × 30 mm × 1.6 mm.

The antenna is fed by CPW and consists of two symmetry planes and a source. By introducing the microstrip transitions between the 50-feed line and Sierpinski gasket fractal, impedance bandwidths can be improved. The optimized dimensions are listed in Table 1.

2.2. Design Process

To better explain the antenna design, Figure 2 shows six evolution stages of the antenna. All the parameters of the antenna are optimized stepwise. During the stepwise optimization, at one time, one parameter is varied while keeping all other parameters constant. The basic or zeroth iteration of the designed antenna structure consists of a square radiator, coplanar waveguide feeding, and partial rectangular ground planes symmetrical to the feed line. From this 18 mm × 18 mm square radiator, a 9 mm × 9 mm square patch is etched away from both upper sides of the antenna. This results in the first iteration of the antenna structure. In the second iteration, from the 9 mm × 9 mm square patch, 4.5 mm × 4.5 mm square patch is etched away. Thereafter, a 4.5 mm × 4.5 mm central square slot is etched out from the first iteration structure to derive the second iterative structure. This pattern is repeated to obtain the structure of remaining iterations.

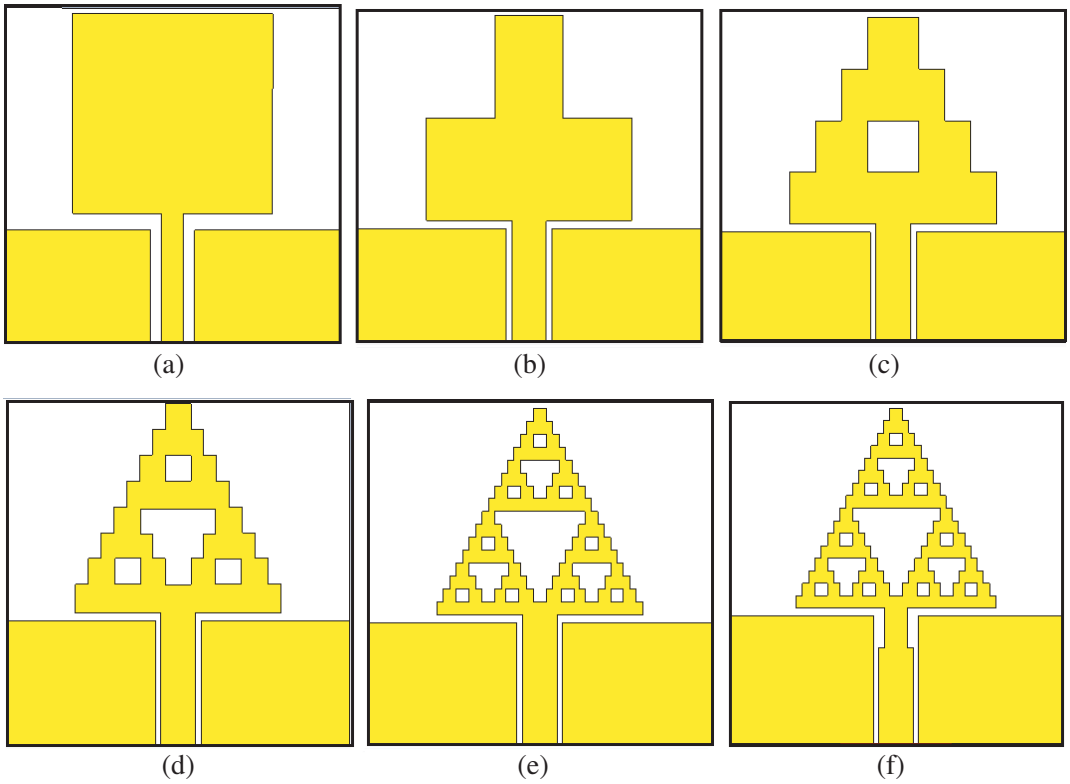

Figure 2. Evolution stages of proposed antenna. (a) Square patch. (b) First iteration. (c) Second iteration (zeroth iteration). (d) Third iteration. (e) Fourth iteration. (f) Final antenna with transition.

Compared to microstrip patch antenna, coplanar waveguide feeding technique has wider bandwidth, better impedance matching, lower radiation loss, and less dispersion [2].

The comparison of intermediated stages in terms of their reflection coefficient characteristics is shown in Figure 3 and listed in Table 2. It is observed that as the number of iterations increases from the zeroth to second, the impedance matching is improved. Zeroth iteration antenna has single resonance frequency, while those from the first to final structures have dual-band characteristics with

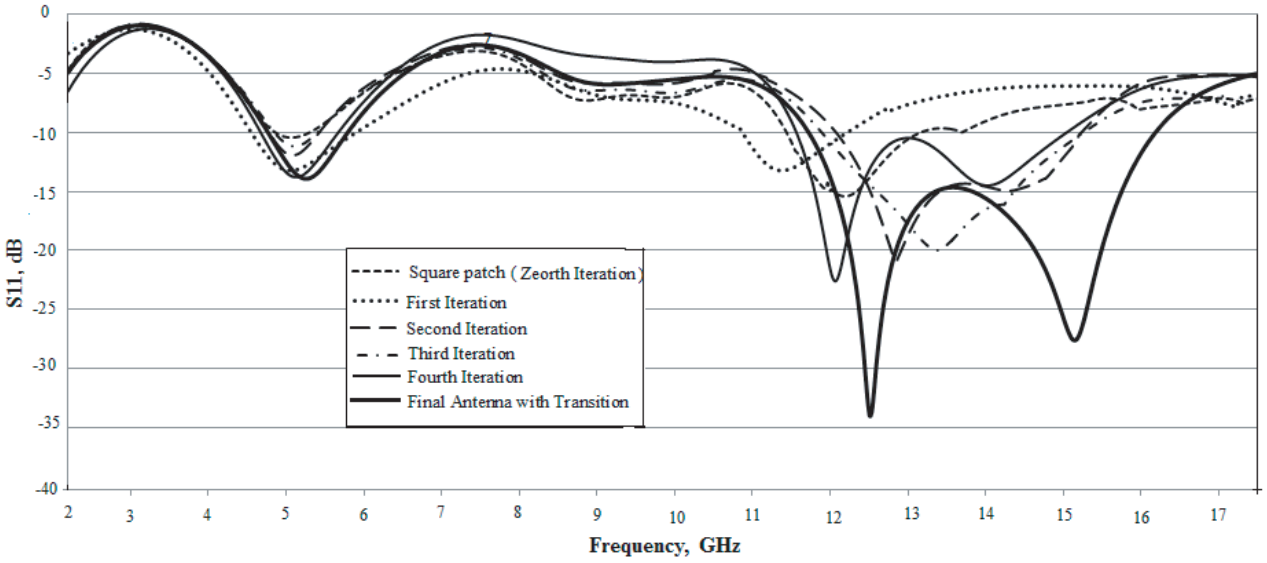

Figure 3. Simulated Reflection coefficient versus frequency characteristics for return loss S_{11} (dB) of antenna evolution stages.

Table 2. Comparisons of four Iterations of the Designed Antenna with the final antenna.

Sl. No.	Iterations	f_L (GHz)	f_H (GHz)	BW (GHz)	f_L (GHz)	f_H (GHz)	BW (GHz)
1	Square Patch (Zeroth)	11.1	12.9	1.8	-	-	-
2	First	3.55	5	1.45	10.5	11.94	1.8
3	Second	3.78	4.45	0.7	11.88	15.44	3.56
4	Third	3.8	4.45	0.65	11.6	15.44	3.84
5	Fourth	3.75	4.91	1.16	11.22	15.36	4.14
6	Final with transition	3.78	4.94	1.16	11.49	16.45	4.96

better impedance matching. The fifth model also possesses dual-band performance, that is, with an improved bandwidth of 1.16 GHz (3.75 to 4.91 GHz) and 4.14 GHz (11.22 to 15.36 GHz) due to the smooth transitions between the radiator and feed line. Due to the insertion of transition in the feed line, the final model shows multiband characteristics with improved bandwidths of 1.16 GHz (3.78 to 4.94 GHz) and 4.96 GHz (11.49 to 16.45 GHz) compared to the fourth model.

It is also observed that the impedance matching is improved during the transition from the zeroth to fourth iterations. For the final iteration, the impedance matching is improved over the operating band leading to a single wide operating band from 11.49 to 16.45 GHz. Thus, the introduction of fractal not only enhanced the overall bandwidth and but also increased the number of resonances.

Figure 4 shows the responses of the proposed antenna (final model with transition) with and without loading the ERR structure in terms of reflection coefficient. From this result, it is evident that MERR loaded Sierpinski square gasket fractal antenna shows multiband characteristics, in which three resonant frequency bands, i.e., 3.08 GHz, 5.81 GHz, and 8.02 GHz, are provided by the metamaterial (MERR) structure.

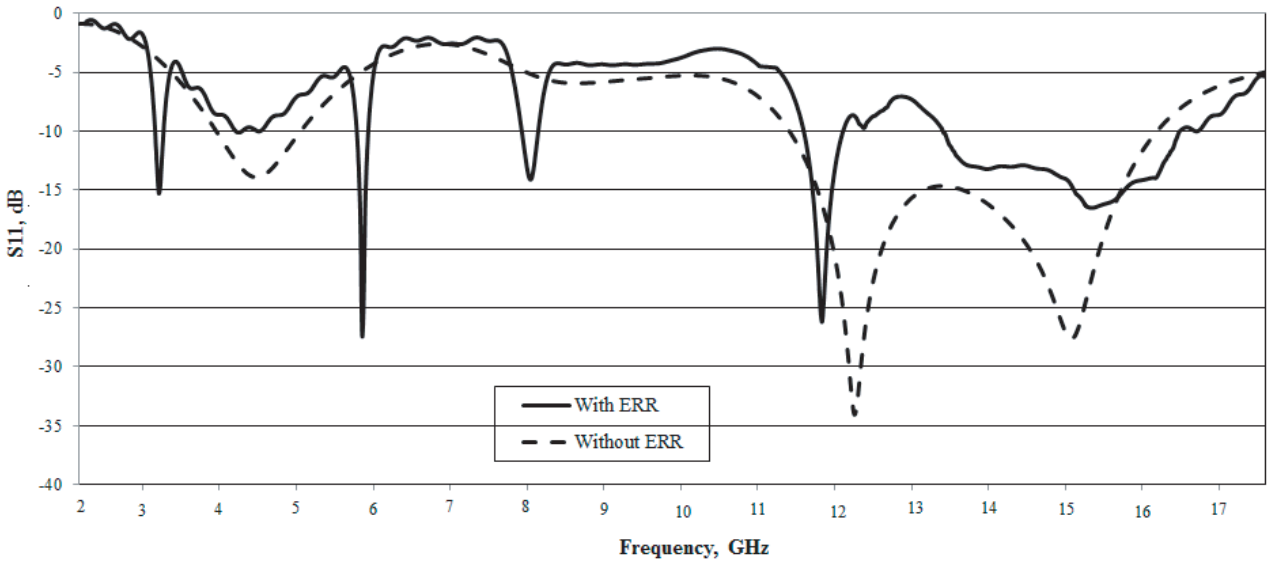

Figure 4. Simulated Return Loss, S_{11} (dB) of antenna loaded with and without ERR.

2.3. Parametric Study

The proposed antenna, as depicted in Figure 1, has many elements that affect its performance. In the following research, when one parameter is changed, the others are kept the same to analyze the influence. To achieve the design requirements, these parameters provide the designer with more degrees of freedom. The most effective parameters will be examined, and their significance on the antenna response will be assessed. In order to analyze the impact of different parameters of the proposed antenna on return loss, we study the variation of S_{11} with different values of G_2, W_f, and L_g when port 1 is excited.

2.4. The Effect of Gap between Radiator and Ground (G_2)

The effect of the variation of the spacing G_2 on the antenna performance is shown in Figure 5, where G_2 is varied from 0.6 mm to 0.9 mm in steps of 0.1 mm. The location of the lower resonant band

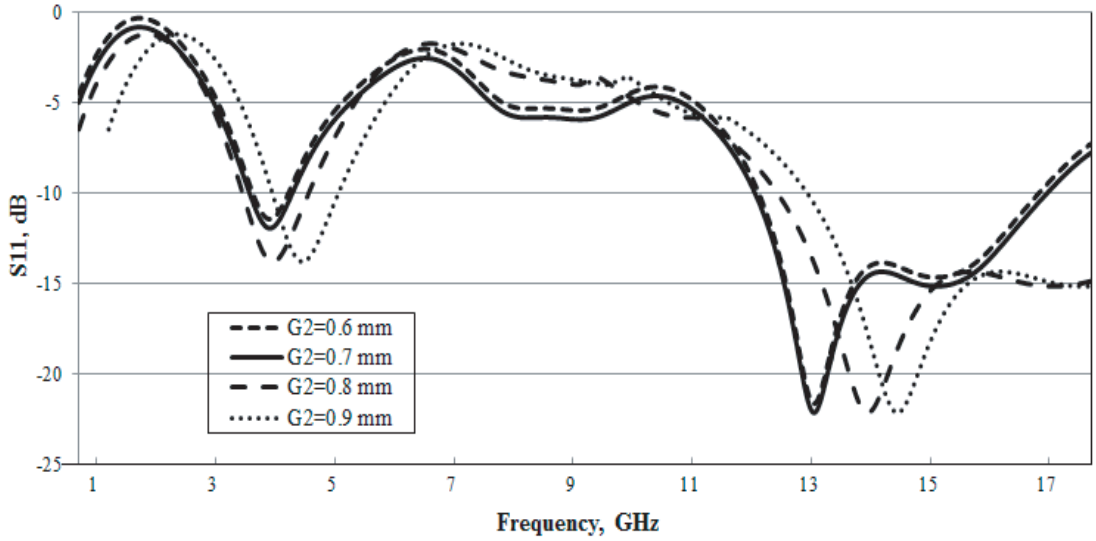

Figure 5. Variation of S_{11}, with different gap width G_2.

and its center frequency are slightly affected. Anyway, the influence on the upper resonant band is more apparent. As gap G_2 increases, the center of the upper resonant band is upshifted while the corresponding bandwidth becomes wider. Above some specific values of G_2, the upper resonant band starts to weaken.

2.5. The Effect of Width of Fedline (W_f)

The effect of the variation of the microstrip feed line width on the antenna performance is shown in Figure 6, keeping the spacing G_2 and other parameters unchanged, where W_f is varied from 3.0 mm to 3.6 mm in steps of 0.2 mm. The lower resonant band is not affected except for the more strengthened coupling of the band. However, the effect on the upper resonant band is more evident. As the width of the fedline increases, the upper resonant band is considerably affected; its position is shifted up while the corresponding bandwidth becomes narrower. Above certain values of fedline width, the upper resonant band starts to diminish.

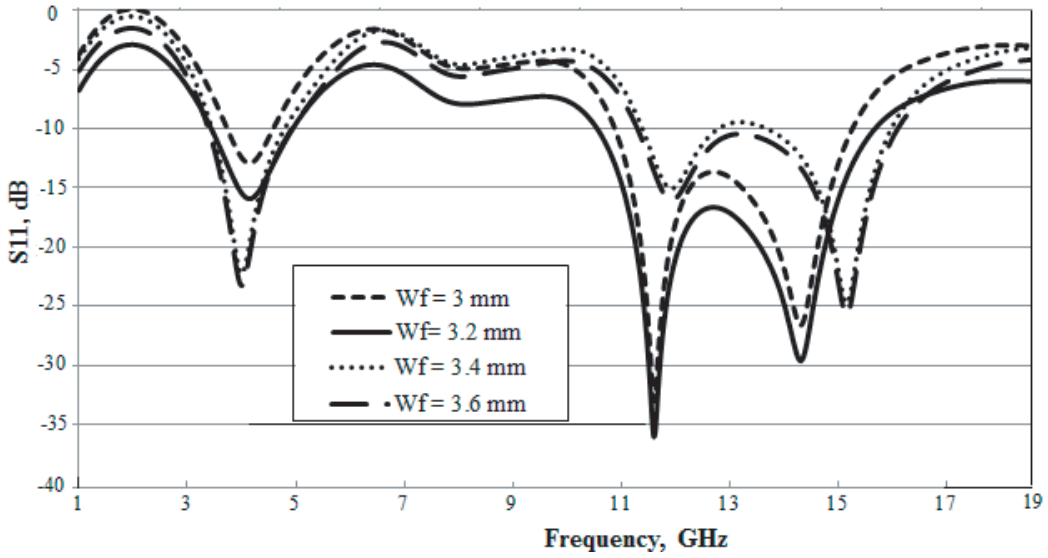

Figure 6. Variation of S_{11}, with different fedline width W_f.

2.6. The Effect of Height of Ground (L_g)

The effect of the variation of height of ground on the antenna performance is shown in Figure 7. The antenna ground plane height is varied from 10.7 mm to 10.9 mm in steps of 0.1 mm. As the height of ground increases, the lower resonant band is slightly affected; its position is shifted down while the corresponding bandwidth is broadened. On the other hand, the upper resonant band is shifted down. However, the variation of the upper resonant band covers a broad frequency range starting from about 3.0 to 5.1 GHz.

2.7. Multi-Mode Electric Ring Resonator (MERR)

As a component of a UWB antenna, the ERR can be used in the design of a metamaterial structure [12, 13]. To realize MERR structure and its equivalent circuit, a tri-mode structure of the ERR providing a passband response at three chosen frequencies is used. The chosen frequency is controlled by the ERR geometry. Schematic diagram of the ERR consists of a square ring with the quasi-lumped capacitance inside. The equivalent diagram of the ERR corresponds to a parallel LC-tank [19, 20]. The resonant frequency depends on the inductance L (ring dimensions) and the capacitance C (the central gap width Gc and length Lc).

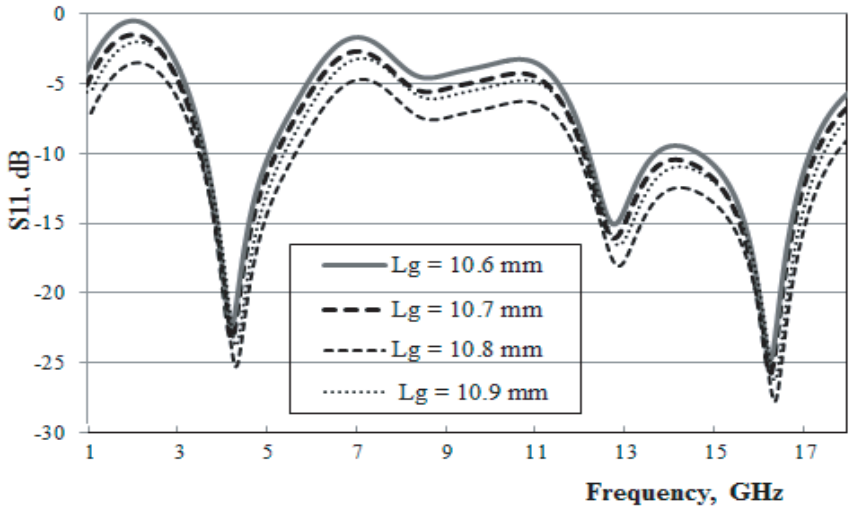

Figure 7. Variation of S_{11}, with different ground height L_g.

The modified structure of the dual-mode resonator (dual-ERR) consists of two nested square rings. The behavior of the resonances at the first and second frequencies of the dual-ERR has been analyzed during the parametric study of the CPW with dual-ERR [14]. The low-frequency mode is provided by the excitation of the central capacitor and inner ring.

The current in the outer ring is conditioned by a mutual inductance between the rings [21]. This means that the resonant frequency of the first mode depends on the dimensions of the inner square ring L_1 and the quasi-lumped capacitance Lc, Gc. The second mode corresponds to the resonant response of the structure formed by two coupled rings with dimensions L_1 and L_2.

The tri-mode ERR (tri-ERR) is used for the design of triple bands, shown in Figure 8. The tri-ERR (TERR) of the antenna contains three coupled rings and a modified interdigital capacitor. The optimized dimensions are listed in Table 3.

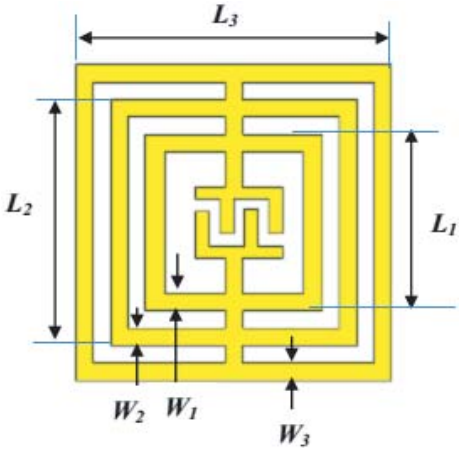

Figure 8. Tri-mode ERR (tri-ERR): Schematic diagram.

The modified interdigital capacitor integrated into the tri-ERR is used for a realization of the first notch at frequency of 3.08 GHz. The low-frequency mode is provided by the excitation of the interdigital capacitor and inner ring. Two other modes arise from the resonances of structures formed by coupled rings with dimensions L_1, L_2, and L_3. Thus, the triple band antenna design starts with the setting of the first mode by properly choosing the geometry of the capacitance and inner ring (L_1); then, the

Table 3. Dimensions of the MERR.

Parameters	Dimensions (mm)	Parameters	Dimensions (mm)
L_1	5	W_1	1
L_2	7	W_2	0.5
L_3	9	W_3	0.5

third mode is set by choosing a proper dimension of the middle ring (L_2), and finally, the second mode is set by choosing a proper dimension of the outer ring (L_3).

For a design of the adjustable UWB triple band antenna based on tri-mode ERR, it is necessary to analyze the equivalent circuit model of such tri-ERR. An equivalent circuit model of the proposed tri-ERR is presented in Figure 9.

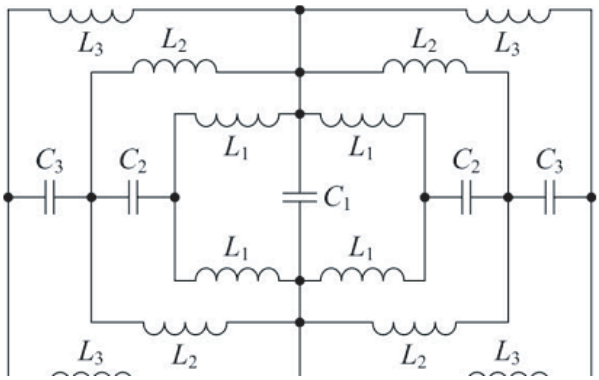

Figure 9. Equivalent circuit model of proposed tri-mode ERR (tri-ERR).

In this paper, the Nicolson Ross Wier process is measured to attain the negative permeability of the proposed MERR. The proposed MERR structure is validated with the negative permeability characteristics by using waveguide method. The proposed multi-mode electric ring structure is placed within waveguide as open in Figure 10(a). The MERR loaded Sierpinski square fractal antenna design has exposed notch in the S_{11} characteristics. The real parts of permeability are extracted as given in Figure 10(b). Thus the metamaterial property proves the effective material constraints.

3. RESULTS AND DISCUSSIONS

3.1. Simulation Results

The simulated results show multiple band operations of the proposed fractal antenna which ranges 3.08/5.81/8.08/12.01/15.58 GHz with VSWR at 1.34/1.12/1.3/1.06/1.56/1.32 which covers S/C/X/Ku band wide bandwidth from 13.55 GHz to 16.79 GHz, useful for IEEE 802.11/WLAN/IEEE 802.16/Wi-MAX applications. To categorize the behaviour of the antennas reverberating method exciting current distributions of the antenna model are shown in Figure 11.

For S-band frequency, 2.5 GHz, current is practically in the feed line as revealed in Figure 11(a). For 3.08 GHz, C band is in the iterated Sierpinski square fractal, and the maximum current density is in MERR as shown in Figure 11(b). At X-band frequency 12.01 GHz, maximum current density is in the edges of the iterated Sierpinski square fractal. The simulated gains of the MERR loaded Sierpinski square fractal antenna are 2.38 dBi, 5.22 dBi, 5.11 dBi, 3.48 dBi, and 5.86 dBi at center frequencies 2.5 GHz, 3.0 GHz, 5.5 GHz, 8 GHz, and 12 GHz, respectively. The simulated gain in 3D pattern is shown in Figure 12.

In Table 4, it is shown that the planned antenna produces superior antenna performance, covering more functional bands than the those in existing literature.

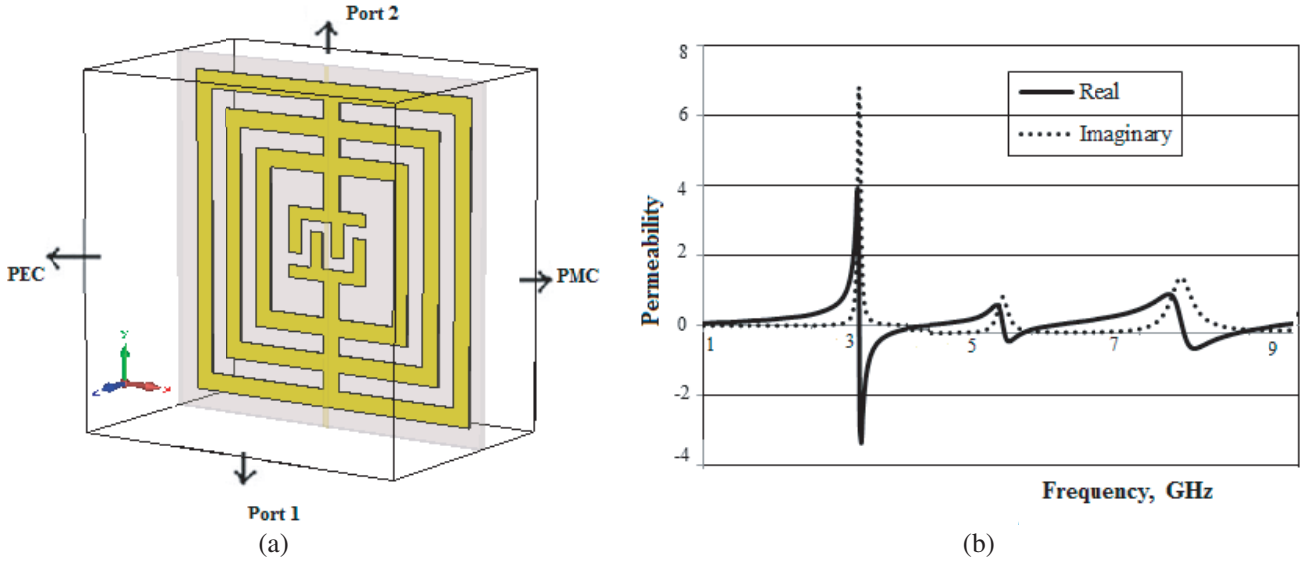

(a) (b)

Figure 10. Waveguide setup for tri-mode ERR (tri-ERR).

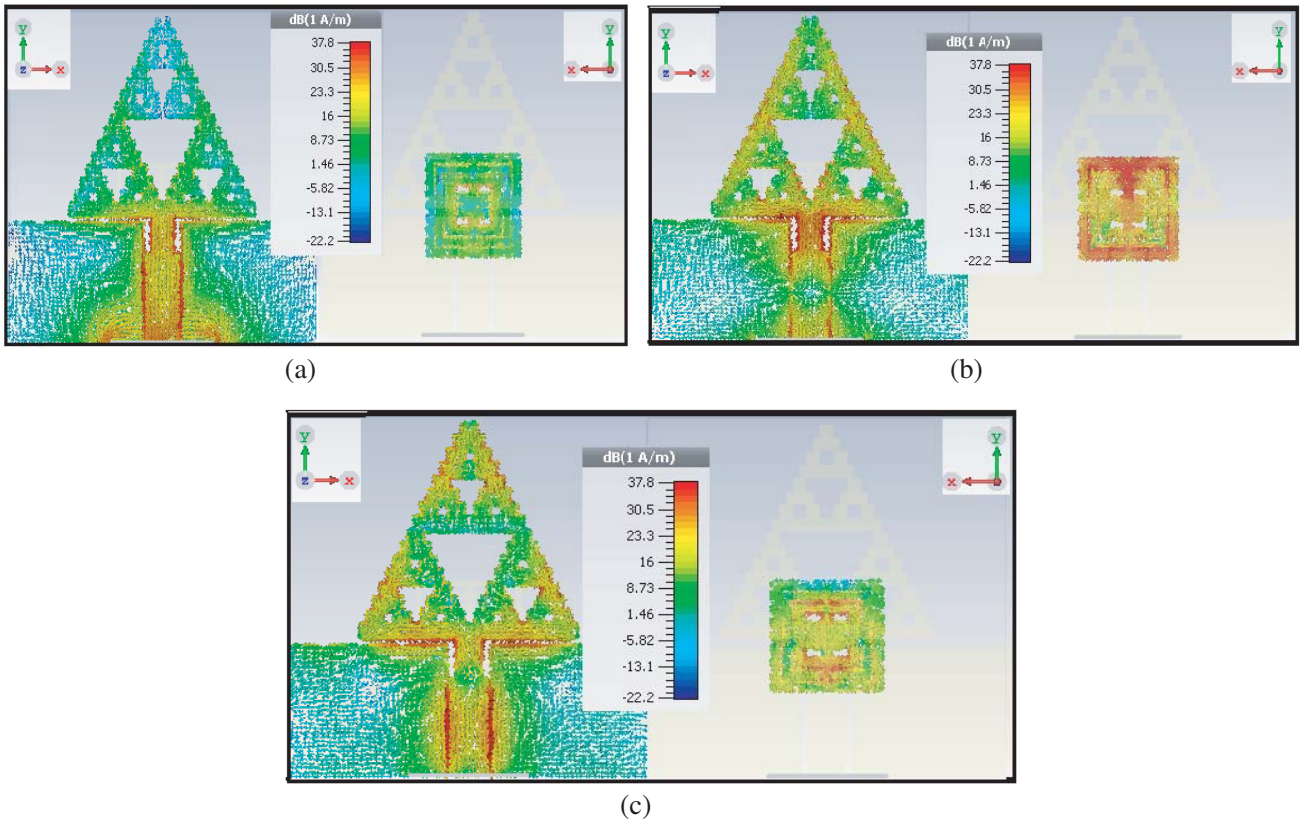

(a) (b)

(c)

Figure 11. Simulated surface current distributions for the antenna projected. (a) 2.5 GHz, (b) 3 GHz, (c) 12 GHz.

3.2. Experimental Results

In order to verify the simulated results, Sierpinski square gasket fractal patch configuration (top view) and Multi-mode Electric Ring Resonator (MERR) is fabricated, measured, and compared. Figures 13(a)

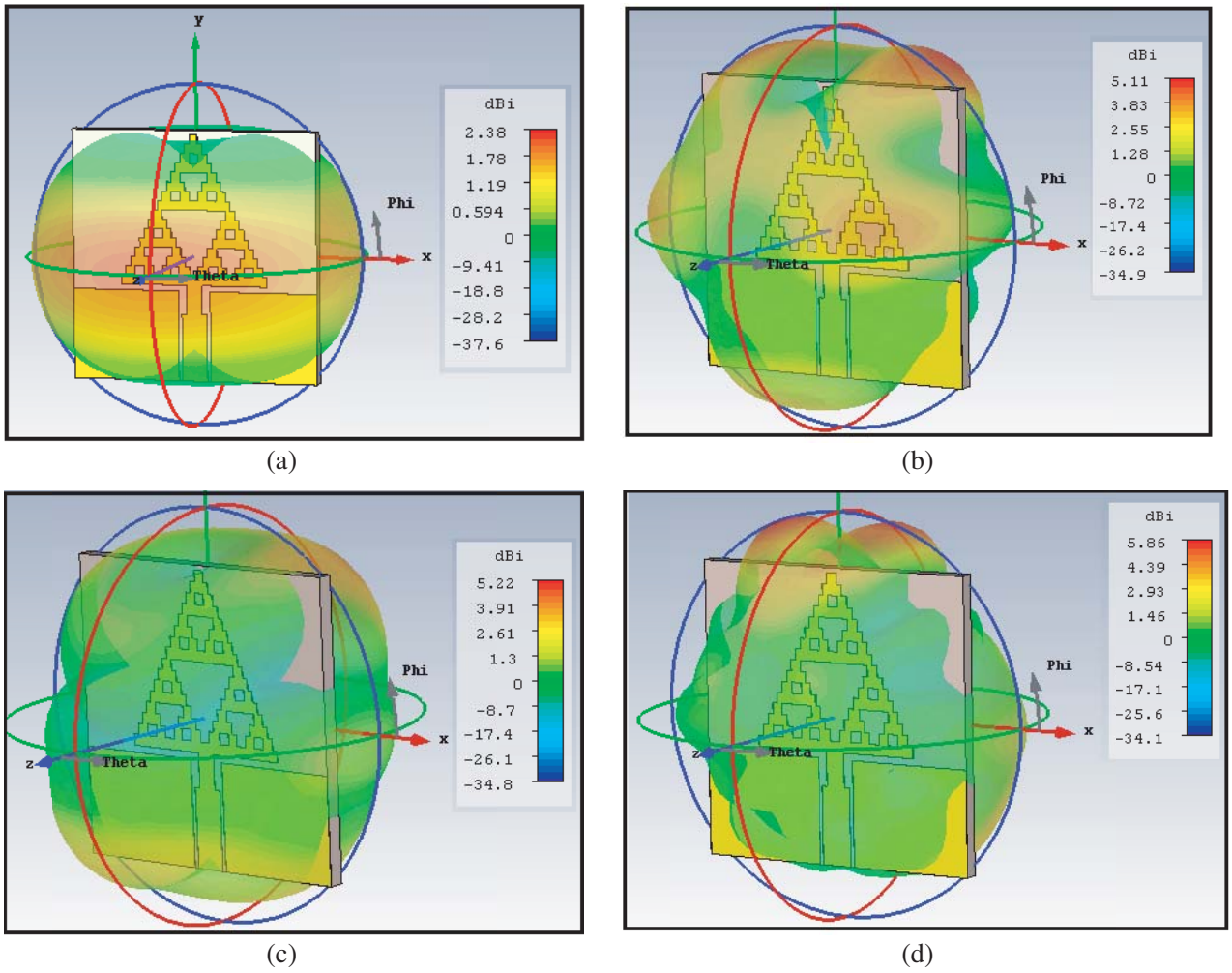

Figure 12. Simulated Gain in 3D pattern. (a) 2.5 GHz, (b) 3 GHz, (c) 5.5 GHz, (d) 12 GHz.

Table 4. Comparison of different existing fractal MM antennas by way of antenna proposed.

Sl. No.	References	Antenna Size (mm^2)	Frequency enclosed (GHz)	Antenna Nature
1	Proposed	30 × 30	3.08/5.81/8.08/12.01/15.58	Muti-band
2	[24]	34 × 51	2.2/4.4/5.8	Tri band
3	[23]	28 × 26	2.6/4.8	Dual band
4	[22]	40 × 40	2.5/5.5	Dual band
5	[28]	25.5 × 25.5	2.45/5.50	Dual band
6	[25]	23 × 10.8	3.60	Single band

and 13(b) show the fabricated antenna with the MERR on the reverse side.

Simulated and measured results show superior agreement of multiple band operations of the MERR loaded Sierpinski square fractal antenna with frequencies 3.08/5.81/8.02/12.13/15.56 GHz which covers S/C/Ku band and shows wide bandwidth characteristics from 13.58 GHz to 16.2 GHz which is useful for WLAN/IEEE 802.16/Wi MAX applications as exposed in Figure 14. The return loss characteristic is measured by using vector network analyzer.

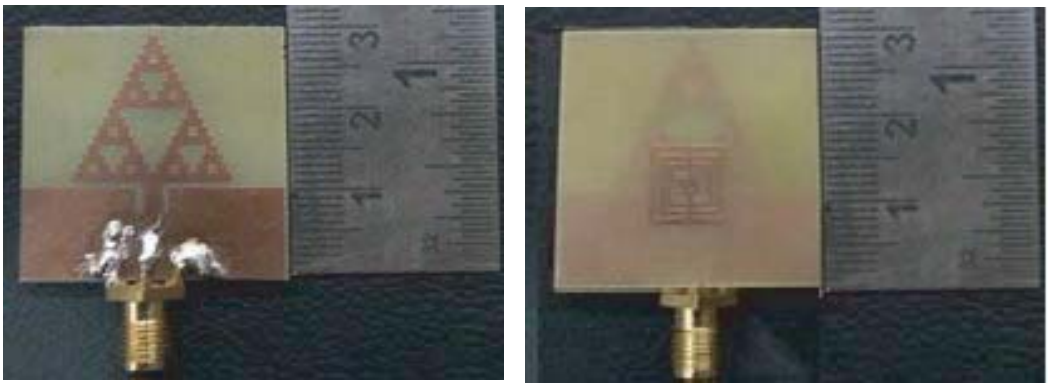

(a) (b)

Figure 13. Snap of the Fabricated MERR loaded Sierpinski square fractal antenna. (a) Top view. (b) Flipside view.

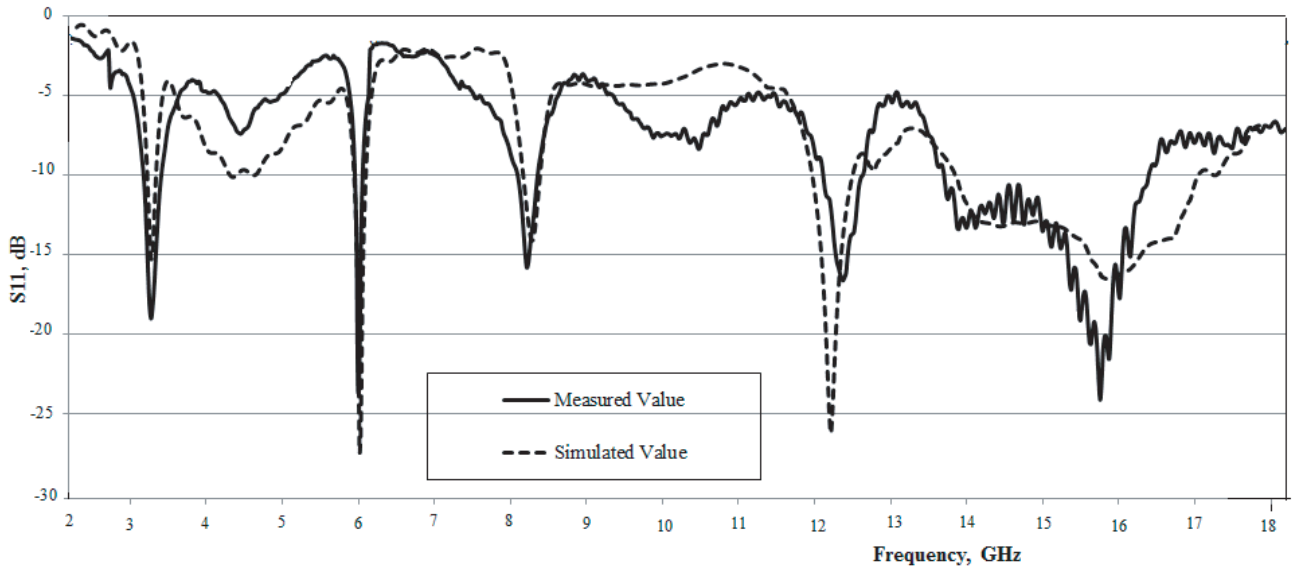

Figure 14. Compared simulated and measured S_{11}.

From Figure 14, it is clear that simulated and experimental results are in good agreement. The discrepancies between the simulated and experimental results can be attributed to the manufacturing tolerances, quality of the SMA connector, and scattering measurement environment. The fabricated MERR loaded SSGF antenna has resonances at frequencies of 3.08/5.81/8.02/12.13/15.56 GHz which covers S/C/Ku band with wide bandwidth from 13.58 GHz to 16.2 GHz. Details of simulated and measured antenna bandwidths at different frequencies are given in Table 5. The graph showing variation of bandwidth at different operating frequencies is given in Figure 15.

The simulated and measured far-field radiation patterns in E- and H-planes of the antenna at the resonant frequencies of 3.08 GHz, 5.81 GHz, and 8.02 GHz are shown in Figures 16(a), (b), and (c), respectively. The results show that omnidirectional pattern is observed in H-plane and bidirectional radiation pattern observed in E-plane. The simulated and measured gains at the resonance frequencies are plotted in Figure 17. The proposed antenna has radiation efficiencies of 89.4%, 95.29%, 79.2%, and 82.64% at the resonance frequencies of 3.08 GHz, 5.81 GHz, 8.08 GHz, and 12.01 GHz, respectively.

Table 5. Simulated and measured parameters.

Sl. No.	Frequency (GHz)		Reflection Coefficient (dB)		Band Width (GHz)	
	SV	MV	SV	MV	SV	MV
1	3.08	3.08	−15.26	−19.1	110 MHz (3.14–3.03 GHz)	120 MHz (3.15–3.03 GHz)
2	5.81	5.81	−27.27	−23.1	100 MHz (5.89–5.76 GHz)	190 MHz (5.92–5.73 GHz)
3	8.08	8.02	−14.06	−15.2	250 MHz (8.2–7.95 GHz)	220 MHz (8.19–7.97 GHz)
4	12.01	12.13	−26.19	−15.77	550 MHz (12.33–11.78 GHz)	380 MHz (12.3–11.92 GHz)
5	15.58	15.56	−16.35	−24.1	3.18 GHz (16.8–13.62 GHz)	2.62 GHz (16.2–13.58 GHz)

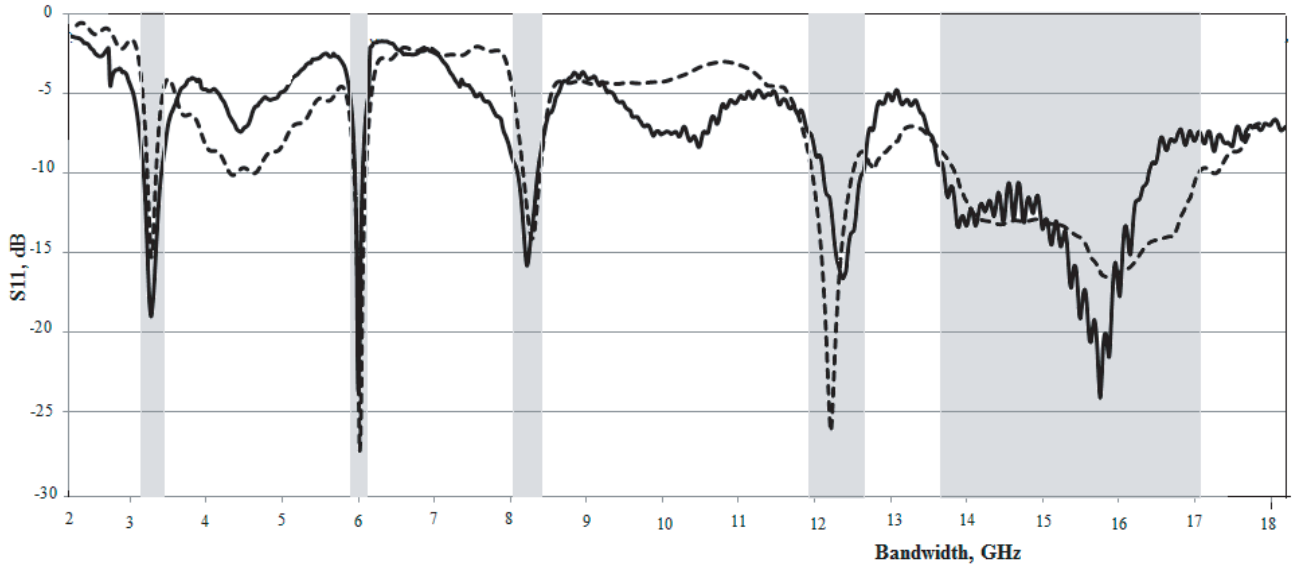

Figure 15. Compared simulated and measured S_{11} with bandwidth.

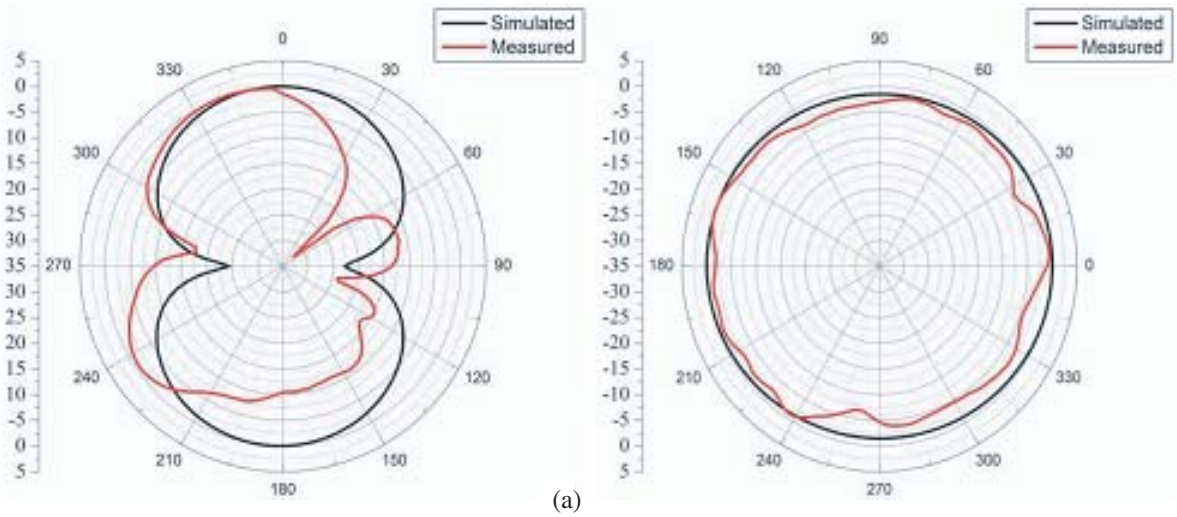

(a)

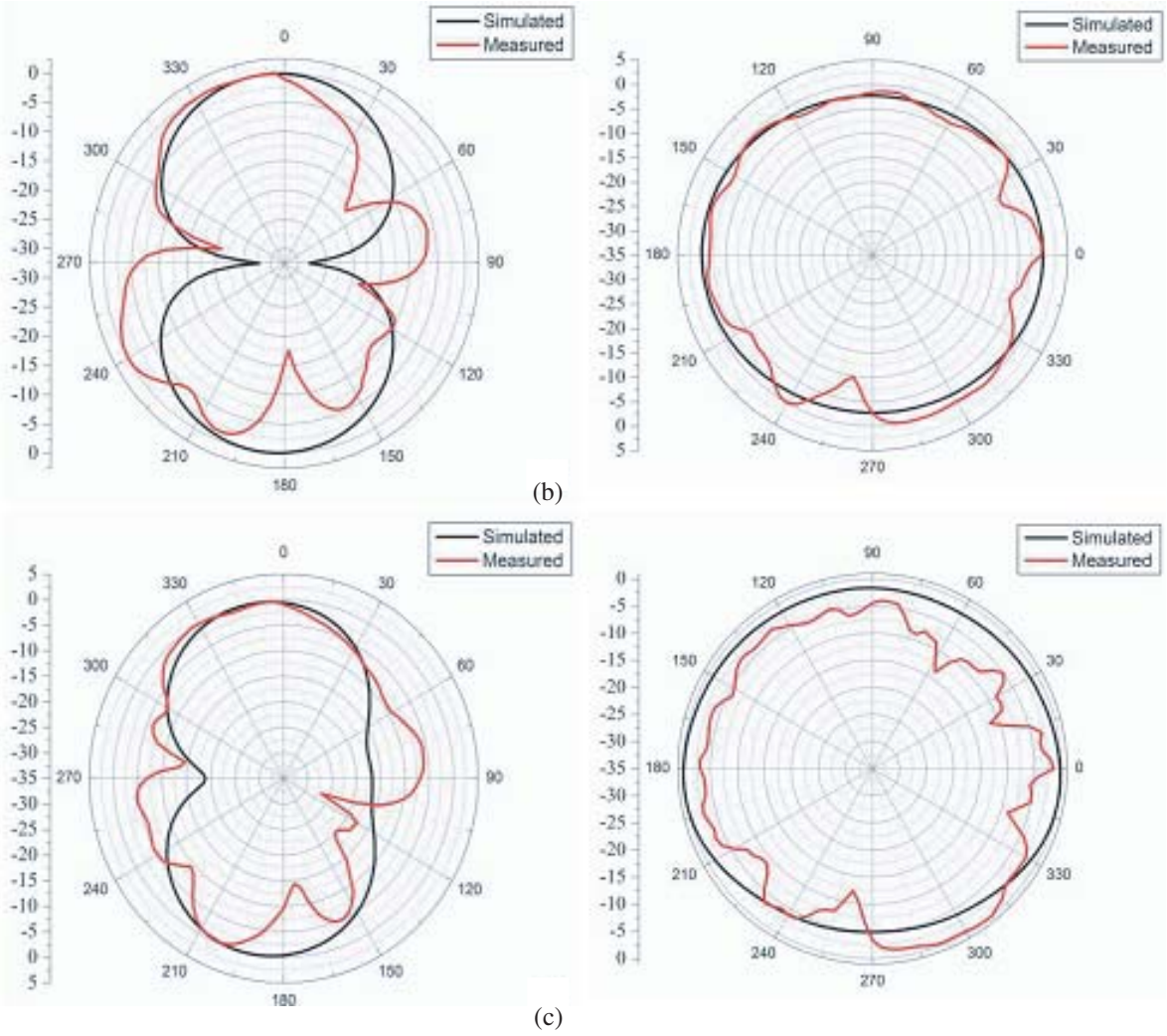

Figure 16. Radiation pattern of proposed antenna at (a) 3.08 GHz, (b) 5.81 GHz, (c) 8.02 GHz. (a) Radiation pattern in E-plane and H-plane at 3.08 GHz. (b) Radiation pattern in E-plane and H-plane at 5.81 GHz. (c) Radiation pattern in E-plane and H-plane at 8.02 GHz.

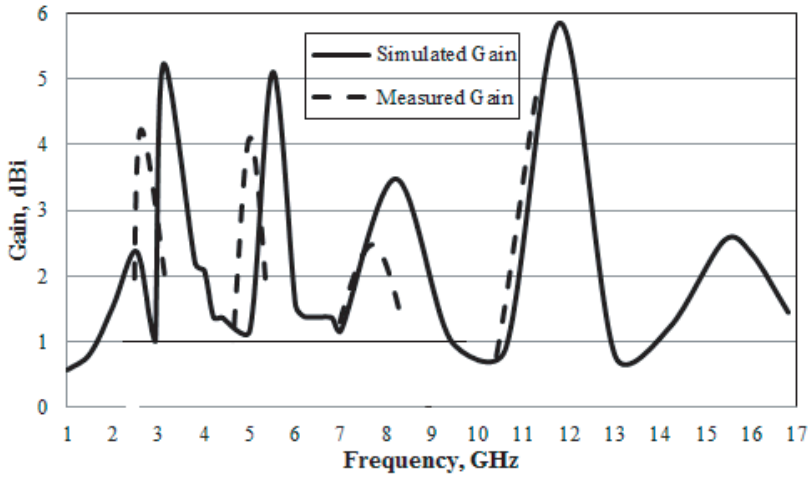

Figure 17. Gain (dBi) of the proposed design over frequency.

4. CONCLUSION

A compact Electric Ring Resonator (ERR) loaded Sierpinski Square Gasket Fractal (SSGF) antenna for multiple frequency band operation has been investigated and thoroughly analyzed in this paper. The proposed antenna size reduction has been carried out on the radiating antenna element and the width of its fed line. The size reduction of the radiating antenna element is achieved by applying the Sierpinski square gasket fractal geometry of four iterations to the radiator side. The conducted parametric study reveals that the antenna will have an exciting performance making it suitable for integration of many of the recently available communication services. A prototype of the proposed antenna is fabricated and tested. Measured results reveal that the antenna offers multiple resonant bands at 3.08/5.81/8.02/12.13/15.56 GHz which cover the frequency spectrum of WiMAX, WiFi/WLAN(IEEE 802.11a), IEEE 802.16e, X-band uplink, S/C/X/Ku, and K band. These multiple band antennas can be smoothly integrated by printed circuit boards (PCBs) of wireless communication devices.

ACKNOWLEDGMENT

The authors would like to thank Dr. C. K. Anandan, H. O. D, Department of Electronics, Cochin University of Science and Technology, Kerala, India for carrying out measurements.

REFERENCES

1. Valagiannopoulos, C. A., "On smoothening the singular field developed in the vicinity of metallic edges," *International Journal of Applied Electromagnetics and Mechanics*, Vol. 31, No. 2, 67–77, 2009.
2. Mahatthanajatuphat, C., S. Saleekaw, P. Akkaraekthalin, and M. Krairiksh, "A rhombic patch monopole antenna with modified Minkowski fractal geometry for UMTS, WLAN, and mobile WiMAX," *Progress In Electromagnetics Research*, Vol. 89, 57–74, 2009.
3. Valagiannopoulos, C. A., "Closed-form solution to the scattering of a skew strip field by metallic PIN in a slab," *Progress In Electromagnetics Research*, Vol. 79, 1–21, 2008.
4. Gupta, M. and V. Mathur, "Koch fractal-based hexagonal patch antenna for circular polarization," *Turkish Journal of Electrical Engineering & Computer Sciences*, Vol. 25, No. 6, 4474–4485, 2017.
5. Valagiannopoulos, C. A., "On examining the influence of a thin dielectric strip posed across the diameter of a penetrable radiating cylinder," *Progress In Electromagnetics Research C*, Vol. 3, 203–214, 2008.
6. Valagiannopoulos, C. A., "Arbitrary currents on circular cylinder with inhomogeneous cladding and RCS optimization," *Journal of Electromagnetic Waves and Applications*, Vol. 21, No. 5, 665–680, 2007.
7. Si, L.-M. and X. Lv, "CPW-FED multi-band Omni-directional planar microstrip antenna using composite metamaterial resonators for wireless communications," *Progress In Electromagnetics Research*, Vol. 83, 133–146, 2008.
8. Nguyen, D. T., H. L. Dong, and C. P. Hyun, "Small planar coplanar waveguide-fed dual band-notched monopole ultra wideband antenna," *Microwave and Optical Technology Letters*, Vol. 53, No. 4, 920–924, 2011.
9. Yu, F. and C. Wang, "A CPW-fed novel planar ultra wideband antenna with a band notch characteristic," *Radio Engineering*, Vol. 18, No. 4, 551–555, 2009.
10. Evangelos, S. A., Z. A. Argiris, I. K. Dimitra, A. A. Antonis, L. Fotis, and D. Kostas, "Circular and elliptical CPW-fed slot and microstrip-fed antennas for ultrawideband applications," *IEEE Antennas and Wireless Propagation Letters*, Vol. 5, No. 1, 294–297, 2006.
11. Poonkuzhali, R., Z. C. Alex, and T. N. Balakrishnan, "Miniaturized wearable fractal-antenna for military application at VHF-band," *Progress In Electromagnetics Research C*, Vol. 62, 179–190, 2016.

12. Gianvittorio, J. P., et al., "Fractal antennas: A novel antenna miniaturization technique and applications," *IEEE Antennas and Propagation Magazine*, Vol. 44, 20–36, 2002.
13. Azari, A., "A new super wideband fractal microstrip antenna," *IEEE Transactions on Antennas and Propagation*, Vol. 59, No. 5, 1724–1727, May 2011.
14. Puente, C., J. Romeu, R. Pous, and A. Cardama, "On the behavior of the Sierpinski multiband fractal antenna," *IEEE Transactions on Antennas and Propagation*, Vol. 46, No. 4, 517–524, 1998.
15. Beigi, P. and P. Mohammadi, "A novel small triple-band monopole antenna with crinkle fractal-structure," *Int. J. Electron. Commun.*, Vol. 70, 1382–1387, Elsevier AEU, 2016.
16. Baena, J. D., J. Bonache, F. Martin, R. M. Sillero, F. Falcone, T. Lopetegi, M. A. G. Laso, J. Garcfa-Farcfa, I. Gil, M. F. Portillo, and M. Sorolla, "Equivalent-circuit models for split-ring resonators and complementary split-ring resonators coupled to planar transmission lines," *IEEE Transactions on Microwave Theory and Techniques*, Vol. 53, 1451–1461, 2005.
17. Bilotti, F., A. Toscano, and L. Vegni, "Design of spiral and multiple split-ring resonators for the realization of miniaturized metamaterial samples," *IEEE Transactions on Antennas and Propagation*, Vol. 55, 2258–2267, 2007.
18. Chang, D. C., B. H. Zeng, and J. C. Liu, "CPW-fed circular fractal slot antenna design for dual-band applications," *IEEE Transactions on Antennas and Propagation*, Vol. 56, 3630–3636, 2008.
19. Schurig, D., J. J. Mock, and D. R. Smith, "Electric-field-coupled resonators for negative permittivity metamaterials," *Appl. Phys. Lett.*, Vol. 88, No. 4, 041109–041109-3, 2006.
20. Withayachumnankul, W., C. Fumeaux, and D. Abbott, "Near-field interactions in electric inductive-capacitive resonators for metamaterials," *Journal of Physics D: Applied Physics*, Vol. 45, No. 48, 485101, Nov. 2012.
21. Rusakov, A., I. Vendik, K. Kanjanasit, J. Hong, and D. Filonov, "Ultra wideband antenna with single- and dual-band notched characteristics based on electric ring resonator," *Proc. Days on Diffraction*, 350–355, St. Petersburg, Russia, Jun. 27–Jul. 1, 2016.
22. Sedghi, M. S., M. Naser-Moghadasi, and F. B. Zarraabi, "A dual band fractal slit antenna loaded by jerusalem crosses for wireless plus WiMAX communications," *Progress In Electromagnetics Research Letters*, Vol. 61, 19–24, 2016.
23. Gorlaa, H. R. and F. J. Haracki-ewicz, "A novel rectangular circle planar monopole ant for ultra wide-band application," *Progress In Electromagnetics Research C*, Vol. 61, 65–73, 2016.
24. Joseph, S., B. Paul, S. Mridula, and P. Mohanan, "A novel Planar fractal antenna with CPW-feed for multiband applications," *Radioengineering*, Vol. 22, No. 4, 1262–1266, 2013.
25. Mishra, N. and R. K. Chaudhary, "A miniaturized ZOR antenna with enhanced bandwidth for WiMAX applications," *Microw. Opt. Tech. Lett.*, Vol. 58, No. 1, 71–75, 2016.
26. Xu, H.-X., G.-M. Wang, Q. Peng, and J.-G. Liiang, "Novel design of triple-band band pass filter based on fractal shaped geometry of a complementary single split ring resonator," *Int. J. Electr. Tay*, Vol. 98, No. 5, 647–654, France, 2011.
27. Adel Abdelrehim, A. and H. G. Shirazz, "Performance improvement of patch antenna using circular split ring resonators and thin wires employing metamaterials lens," *Progress In Electromagnetics Research B*, Vol. 69, 137–155, 2016.
28. Saputro, S. A. and J.-Y. Chung, "Hilbert curve fractal antenna for dual on- and off-body communication," *Progress In Electromagnetics Research Letters*, Vol. 58, 81–88, 2016.
29. Elavarasi, C. and T. Shanmuganantham, "Parametric analysis of water lily shaped SRR loaded fractal monopole antenna for multiband application," *WASET Int. J. Electr. Comp. Energetic Electro Comm. Eng.*, Vol. 10, No. 9, 2016.